Sang Yeop Han, Ray R. Taghavi and Saeed Farokhi*

Passive Control of Supersonic Rectangular Jets through Boundary Layer Swirl

Abstract: Mixing characteristics of under-expanded supersonic jets emerging from plane and notched rectangular nozzles are computationally studied using nozzle exit boundary layer swirl as a mean of passive flow control. The coupling of the rectangular jet instability modes, such as flapping, and the swirl is investigated. A three-dimensional unsteady Reynolds-Averaged Navier-Stokes (RANS) code with shock adaptive grids is utilized. For plane rectangular nozzle with boundary layer swirl, the flapping and spanwise oscillations are captured in the jet's small and large dimensions at twice the frequencies of the nozzles without swirl. A symmetrical oscillatory mode is also observed in the jet with double the frequency of spanwise oscillation mode. For the notched rectangular nozzle with boundary layer swirl, the flapping oscillation in the small jet dimension and the spanwise oscillation in the large jet dimension are observed at the same frequency as those without boundary layer swirl. The mass flow rates in jets at 11 and 8 nozzle heights downstream of the nozzles increased by nearly 25% and 41% for the plane and notched rectangular nozzles respectively, due to swirl. The axial gross thrust penalty due to induced swirl was 5.1% for the plane and 4.9% for the notched rectangular nozzle.

Keywords: passive control, supersonic jets, rectangular nozzles, shear layer swirl, jet instabilities

***Corresponding author: Saeed Farokhi:** Department of Aerospace Engineering, University of Kansas, Lawrence, Kansas 66045, USA
E-mail: sfarokhi@ku.edu
Sang Yeop Han: Propulsion Control Department, Korea Aerospace Research Institute, Daejeon 305-333, South Korea
Ray R. Taghavi: Department of Aerospace Engineering, University of Kansas, Lawrence, Kansas 66045, USA

1 Introduction

The interest in high-speed jet mixing enhancement stems from an expected improvement in combustion efficiency in scramjet engines to jet noise reduction in supersonic aircraft and signature reduction for military vehicles. One solution that has been considered is the excitation method that promotes the growth of the most unstable modes, which in turn leads to large-scale jet mixing enhancement. Here we distinguish between macroscopic mixing and the molecular level mixing enhancement in a jet, where the latter is the most suitable characteristic in combustion research. In this paper, we study macroscopic or large-scale mixing enhancement in a supersonic jet due to swirl. Jet excitation may be accomplished either actively through internal/external acoustic excitation or mechanical vibration of flaps or tabs among other means – or passively – through geometrical alteration of the nozzle exit plane. The passive control methods are less complex, incur less system weight and are less costly than their active counterparts.

In the current study, a swirling shear layer is induced at the nozzle exit plane which acts as a passive means of flow control. Swirling flows are widely applied to the design of various combustion chambers, spray nozzles, environmental units, among others. In liquid rocket engines and aircraft combustion chambers, swirl is induced in the injected propellants or fuel respectively as a means of flame stabilization and combustion efficiency improvement [11]. The change of nozzle exit configuration for passive jet excitation control has already proven to be effective in mixing enhancement by previous researchers [6, 10, 12, 13, 15, 18–21, 29, 33].

Jet excitation for the purpose of mixing enhancement usually induces turbulence in the shear layer, which leads to byproducts such as supersonic jet noise, broadband shock associated noise, and screech tones. The characteristics of both mixing and shock-associated noises can be predicted by examining supersonic jet flowfield as the noise source is embedded in supersonic jet plume as discussed by Kim et al. [17], Lo et al. [22], Raman [26], and Raman and Rice [27]. To analyze and investigate noise sources, the instability modes, which are well-known as the sources of supersonic jet noise, should be carefully observed experimentally or accurately simulated computationally.

Previous experimental studies indicate that swirl has large-scale effects on flowfields such as jet growth, mixing enhancement, flame size, shape, stability, and

combustion intensity [26, 27, 32, 33]. Also computational methods have been applied in finding a control strategy for mixing enhancement and noise reduction while the mechanism and phenomena of mixing and shock-associated noise in supersonic jets are examined [7, 17, 22]. Supersonic jets issuing from convergent-divergent nozzles were examined experimentally by Suda et al. [32] with a plane rectangular nozzle with high aspect ratio to simulate two-dimensional jets. Two modes of jet oscillations, namely flapping and symmetrical oscillation modes ($f_{symmetrical} \approx 2f_{flapping}$) were observed in their results. They also observed the dynamic behavior and traveling wave, which was the dominant source of screech noise generation, inside the third shock cell in the flapping mode. Raman and Rice [27] examined the evolution of hydrodynamic instability modes, which are self-excited by harmonically related natural screech tones using a convergent rectangular nozzle with an aspect ratio of 9.63 in supersonic jet. They also observed strong three dimensionalities beyond $x/h = 7$ in the coherent wave evolution in both streamwise and spanwise directions. In the review paper on supersonic jet screech tones by Raman [26], he pointed out that the instability modes in shock containing jets such as oscillation mode, shock-cell spacing, and unsteady shock motion were related to both screech noise and broadband shock-associated noise. A passive approach to excite a free jet with tabs at nozzle exit lip was examined experimentally by Behrouzi and McGuirk [6] for an under-expanded supersonic rectangular jet, and Ibrahim and Nakamura [15] for a circular nozzle with jet exit Mach number of 1.33. Ibrahim and Nakamura used two types of vane tabs – stationary and rotatable – placed at diametrically opposite locations along the circumference of circular supersonic jet nozzle exit as vortex generators. They observed that vane tabs generated streamwise vortices, which caused a more rapid spread rate than a plane jet. Also it was noted that rotating tabs caused the jet to decay faster than stationary tabs since the rotation of streamwise vortices influenced the jet spread rate more than the steady streamwise vortices.

Kim et al. [17] performed computational study using PARC code with a k-ε turbulence model on the essential noise related flow quantities such as turbulence intensity and shock strength. They found from their study that shock strength was not the major contributor in turbulent mixing noise. LES method with TVD and WENO characteristic filters and a sixth-order compact scheme to capture shocks was also used for numerical investigations on supersonic jet noise prediction with the fully expanded and under-expanded supersonic jet flows of 1.95 Mach number [22] and 1.3 Mach number [7]. The effect of jet excitation method was studied computationally by Kolbe et al. [21] with paddles in the flowfield of supersonic rectangular jet. The paddles caused strong flapping motions and resulted in jet mixing enhancement. With paddles located at $x/h = 7.3$, they estimated the flapping frequency of 4700 Hz with the amplitude of 147.5 dB at nozzle lip, which agreed very well with the experimental results of Rice and Raman [29]. The effects of paddles on the heated supersonic rectangular jets were also studied numerically by Kolbe et al. [20]. Their simulations showed that the development of shear layer in the heated jets took more time than the unheated jet (300 K). They also found that the mode at the lower frequency was varicose and the higher frequency mode was sinuous, which suggests that the significant change occurred with the heated jet as compared to the unheated jet.

In this paper, authors computationally examined the large scale mixing characteristics and the behaviors of jet instabilities for under-expanded supersonic jets emerging from plane and 45° notched rectangular nozzles. The nozzle aspect ratio is 5 and it is under expanded with choked exit condition. The fully-expanded jet Mach number is 1.526. The nozzle exit boundary layer swirl is set at 30° in counter-clockwise direction with a swirl number of $S = 0.41$. The computational prediction of supersonic jet noise requires a code, which can accurately simulate the mean flow structure and interaction of jet's under/overexpansion shocks with the turbulent mixing layer. For the detailed simulation of supersonic jet noise, a direct numerical simulation (DNS) with a grid system, which can resolve high wave number energy, or a large eddy simulation (LES) with the well-posed sub-grid scale stress model [7, 22] should be used. However, previously it has been reported that three-dimensional unsteady Reynolds-Averaged Navier-Stokes (RANS) code with a suitable turbulence model is sufficient for computing the supersonic jet flowfields [17]. For the precise simulations on the microscopic behaviors of supersonic jets expensive computations with schemes and grid systems, which can resolve high energy eddies, should be performed [22, 7]. However, the results of the current research will show that computational analysis using Reynolds-Averaged Navier-Stokes (RANS) code with shock adaptive grids and a combination of turbulence models is good enough to simulate the macroscopic behaviors of jet instabilities and mixing characteristics of under-expanded supersonic jets with the effects of boundary layer swirls.

2 Computational Fluid Dynamics (CFD)

For the study of characteristics of supersonic rectangular jets, a computational code *Proteus* [34] was used with a shock-adaptive grid generator developed by authors. The code uses three-dimensional compressible full Navier-Stokes equations in strong conservative form, using vector notation in Cartesian coordinates, as the governing equations. For turbulent flows equations are in the Reynolds time-averaged form of Navier-Stokes equations with density fluctuation neglected. The governing equations are solved by marching in time with the generalized scheme of Beam and Warming [5]. Also the fluid is treated as perfect gas.

Several options of boundary conditions, which are treated implicitly, are available in the code. These boundary conditions are used after being linearized. In this code, numerical boundary reflections are treated carefully by using upwind space differencing scheme only for the velocity derivatives, which have the same direction as velocity terms at the boundary such as du/dx, dv/dy, and dw/dz. For other spatial derivatives, the central differencing scheme is used. The governing equations are solved by an alternating direction implicit (ADI) method, which is used with the appropriate factorization approach, with the boundary conditions specified for all computational domain boundaries; $\xi = 0$ and 1, $\eta = 0$ and 1, and $\zeta = 0$ and 1 planes.

In high Reynolds number flows the odd-even decoupling produced by second order central differencing for the inviscid terms leads to oscillations. Artificial viscosity is normally added to the solution algorithm to suppress high frequency oscillations, which occur in phenomena such as shock waves when they are captured by the finite difference algorithm. The code has two artificial viscosity options; constant model [31] and nonlinear model [16].

The constant model for artificial viscosity has both explicit and implicit artificial viscosities. The standard explicit smoothing uses the fourth order differences, and damps the high frequency nonlinear instabilities. Also the second order explicit smoothing is provided in the code, which gives more smoothing than the fourth-order smoothing. The implicit smoothing is the second order difference and extends the linear stability bound of fourth order explicit smoothing. The nonlinear model for artificial viscosity is strictly explicit. The explicit and implicit artificial viscosities are applied in computation algorithm, which is added in the solution procedure of ADI method. Artificial damping is controlled by adjusting artificial viscosity coefficients – $\varepsilon_E^{(2)}$ for the second-order and $\varepsilon_E^{(4)}$ for the fourth-order; ε_I for the implicit artificial viscosity.

Turbulence models used in the simulations of current study are Baldwin-Lomax [1] and Chien k-ε [9] turbulence models, which have been utilized with the following two-step strategy in simulations:

1. First, from the initial conditions defining supersonic nozzle jet with pressures and velocities at nozzle exit and quiet space with ambient conditions, Baldwin-Lomax turbulence model is used to detect large pressure gradients in plane jet flowfield, which identifies the location of the shock waves in the under-expended jet flow.
2. Second, using the results of the first step as initial conditions, the simulation proceeds with Chien k-ε turbulence model, which refines shock waves and the flowfield in the final solution.

The current study focuses on the exploration of macroscopic phenomena of rectangular supersonic jets such as jet oscillations and large-scale mixing rather than the molecular-level or fine mixing characteristics of supersonic jets. Hence Baldwin-Lomax turbulence model is selected to simulate macroscopic motion of rectangular supersonic jets since it has been recognized as a suitable turbulence model for fast simulations while keeping the solutions reasonably accurate and where the robustness and reliability of simulations are more important than the detailed flow physics [1, 3, 8, 23].

After obtaining the macroscopic physical motions of rectangular supersonic jets by Baldwin-Lomax turbulence model, Chien k-ε turbulence model is used to enhance shock waves which are characterized by large pressure gradients. The k-ε turbulence model produces more accurate results than other turbulence models in the case of plane jet and is useful for free shear layer flows with relatively small pressure gradients [2]. This turbulence model is good for the current simulation because it deals with only small pressure gradients near shock waves and free shear layers where large pressure gradients have been already embedded in the initial flow fields.

3 Nozzle configuration and grid generation

One of the effective methods for the passive flow control of supersonic jets is by placing a series of swirl vanes in the boundary layer at nozzle exit [10]. These nozzle configurations are investigated as effective tools for the mixing enhancement of supersonic jets.

The convergent nozzles that are used in this study are plane and 45° notched rectangular as shown in Figures 1(a) and 1(b). Swirl is induced at 30° angle in the counter-clockwise direction (as viewed from the jet looking upstream at the nozzle exit). Both nozzles have the aspect ratio of 5.0. Experimental studies using the above nozzles without boundary layer swirl have been carried out by other researchers [10, 25, 28].

Due to the three-dimensional nature of the flow, full three-dimensional computational domains are used in both cases as shown in Figures 2(a) and 2(b). The computational grid systems for this study are also shown in Figures 2(a) and 2(b) for the plane and notched rectangular nozzles by using a shock adaptive grid generator, respectively. The initial computational grid system is analytically generated according to the following steps:

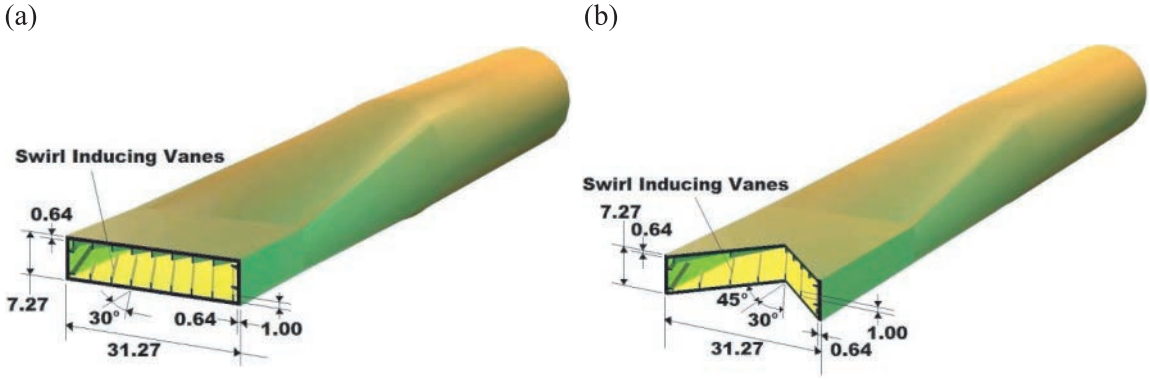

Fig. 1: Nozzle configurations: (a) Plane rectangular nozzle, (b) Notched rectangular nozzle. (Dimensions in mm)

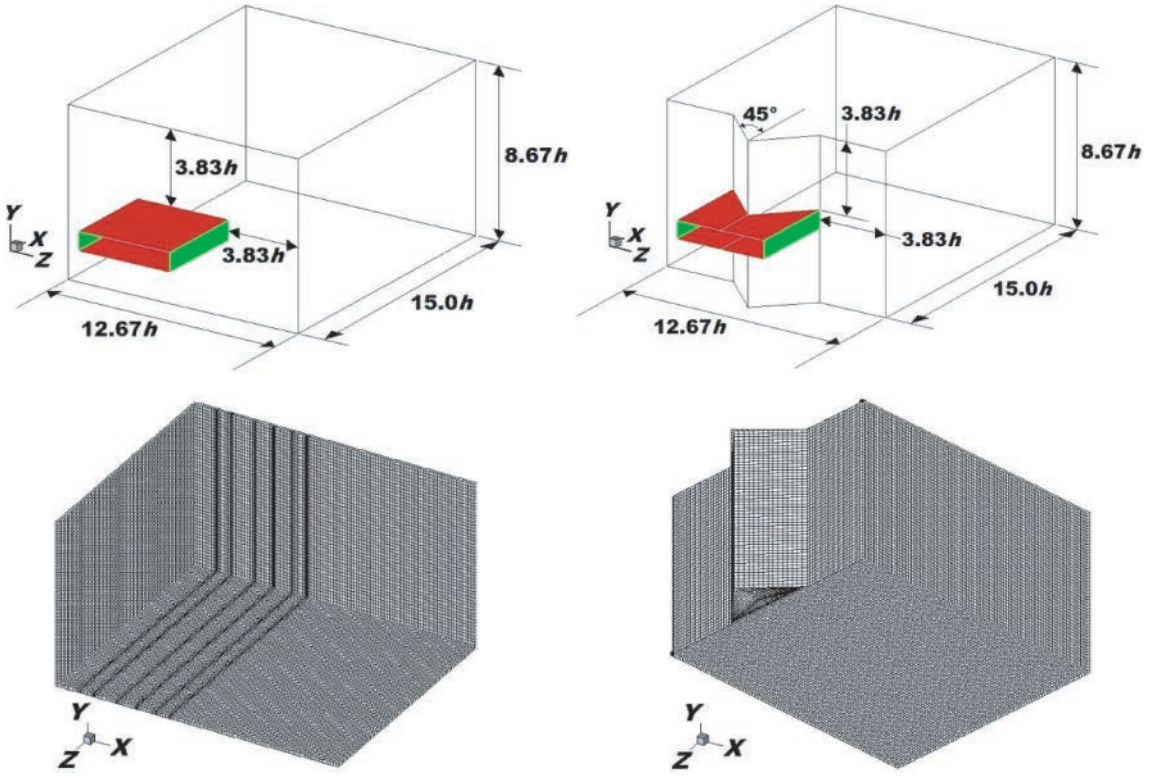

(a) 144 x 53 x 77 (b) 121 x 53 x 77

Fig. 2: Computational domains and adaptive computational grid systems: (a) Plane rectangular nozzle, (b) Notched rectangular nozzle

1. The length (L_x), height (L_y), and width (L_z) of physical domain are divided using the number of grid points – N, M, and P – to get Δx, Δy, and Δz with the following equations:

$$\Delta x = L_x/(N-1) \quad (1)$$

$$\Delta y = L_y/(M-1) \quad (2)$$

$$\Delta z = L_z/(P-1) \quad (3)$$

2. Each grid point is given with physical coordinate (x_n, y_m, z_p) with the following equations:

$$x_n = (n-1)\Delta x \quad \text{where } n = 1 \ldots N, \quad (4)$$

$$y_m = (m-1)\Delta y \quad \text{where } m = 1 \ldots M, \quad (5)$$

and

$$z_p = (p-1)\Delta z \quad \text{where } p = 1 \ldots P. \quad (6)$$

After the initial computation is executed to detect shock locations with a grid system obtained from the above steps, a grid packing procedure is applied for shock adaptive grid with the following procedure:

1. Find each shock location and coordinate (e.g. ($x_{s(0)}$, $y_{s(0)}$, $z_{s(0)}$)) from the results of initial computation;
2. Assign the neighboring grid points using packing rate, R_p%, with the following equations:

$$x_{s(1)} = x_{s(0)} + \Delta x R_p\%, \quad (7)$$

$$x_{s(n)} = x_{s(n-1)} + (x_{s(n-1)} - x_{s(n-2)})(1 + R_p\%), \quad (8)$$

$$x_{s(-1)} = x_{s(0)} - \Delta x R_p\%, \quad (9)$$

and

$$x_{s(-n)} = x_{s(-(n-1))} + (x_{s(-(n-2))} - x_{s(-(n-1))})(1 + R_p\%) \quad (10)$$

where $n = 2 \ldots N$.

3. Continue Step 2 until the interval lengths of neighboring grid points are equal to or more than Δx, Δy, or Δz.

The initial computations are executed with the rectangular structured grid systems, which have the grid size of $61 \times 53 \times 77$. Grid spacings used in the initial computations are $\Delta x = 0.25$ h and $\Delta y = \Delta z = 0.167$ h, which are based on the time step determined by the frequency of instability modes and *CFL* number used in calculations. After the initial computations, a shock adaptive grid generator is applied to the results of initial computations. A shock adaptive grid generator locates shocks from the initial computational results and then generates grids at 20% packing rate at nozzle centerline shock locations as shown in the above figures. Shock adaptive grid systems have grid sizes of: a) Plane rectangular nozzle: $144 \times 53 \times 77$; b) Notched rectangular nozzle: $121 \times 53 \times 77$. With the shock adaptive grid systems, additional computations are performed for the final results.

To minimize the thrust penalty, the height of swirl region at the nozzle exit plane is limited to about 33% of nozzle height or about 6.7% of nozzle width. With this level of embedded swirl in the nozzle boundary layer, the axial thrust penalty is about 5.1% for the plane rectangular nozzle and nearly 4.9% for the notched rectangular nozzle.

4 Boundary conditions

Boundary conditions for both cases are selected such that boundaries except nozzle exit and nozzle wall have zero gradients for pressure and velocity [24]. In addition, the choked nozzle exit plane has pressure, temperature, velocity, and flow angle specified as:

- *Reference conditions:*
  - Pressure: Corresponding to fully expanded Mach number of 1.526
  - Nozzle exit Mach number: 1.0
  - Temperature: 249.85 K
  - Density: 1.414 kg/m^3
- *Boundary conditions:*
  - $\xi = 0$: Nozzle exit: $p = 2.014$, $u = 1.0$, $v = w = 0.0$
    Nozzle wall: No-slip and adiabatic wall
    Outside: Subsonic inflow with zero gradient
  - $\xi = 1$: Supersonic outflow with zero gradient
  - $\eta = 0{,}1$; $\zeta = 0{,}1$: Subsonic outflow with zero gradient
- *Swirl characteristics:*
  Swirl vanes (depth = 1.0 mm) are installed inside nozzle exit to create a counter-clockwise swirl in the jet by tilting vanes by 30° in the clockwise direction at top wall, 30° counter-clockwise-tilt at bottom wall, 30° upward-tilt at left side wall, and 30° downward-tilt at right side wall as shown in Figures 1(a) and 1(b). Instead of simulating vane at the exit boundary inside nozzle, the flow deflection at the exit boundary inside nozzle is implemented. Thus, the following boundary conditions are assigned on grid points where the

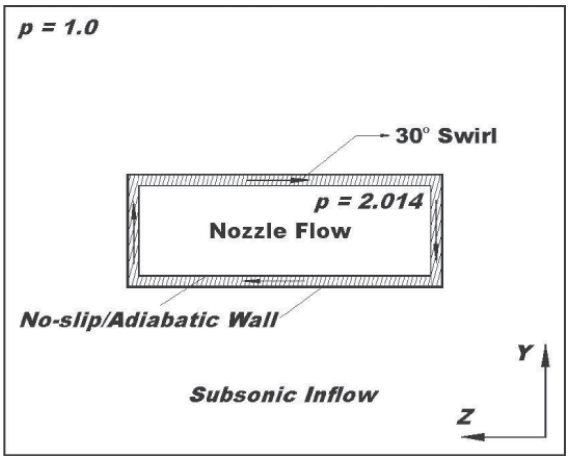

Fig. 3: Boundary conditions at $\xi = 0$ plane

boundary layers swirl resides in $\xi = 0$ plane, the following boundary conditions are assigned as shown in Figure 3:

Inside boundary layer:

Top: $p = 2.014$, $u = \cos 30°$, $v = 0.0$, $w = \sin 30°$

Bottom: $p = 2.014$, $u = \cos 30°$, $v = 0.0$, $w = -\sin 30°$

RHS: $p = 2.014$, $u = \cos 30°$, $v = \sin 30°$, $w = 0.0$

LHS: $p = 2.014$, $u = \cos 30°$, $v = -\sin 30°$, $w = 0.0$

Here, the degree of swirl (or swirl number), S, is defined as:

$$S = (w_{max}/u_{max})/(2 - (w_{max}/u_{max})) \qquad (11)$$

where $w_{max} = \sin 30°$ and $u_{max} = \cos 30°$. Thus the degree of swirl in the jet becomes $S = 0.41$ for 30° counter-clockwise boundary layer swirl.

In addition to the above conditions, artificial damping is applied to both supersonic computations with the following fourth-order explicit and second-order implicit artificial viscosities using the constant coefficient model of Steger [31] – 4th-order explicit artificial viscosity coefficient, $\varepsilon_E^{(4)} = 0.50$; 2nd-order implicit artificial viscosity coefficient, $\varepsilon_I = 1.00$.

5 Results and discussions

On the effect of swirl, which may be induced in a jet by employing swirl vanes, the centrifugal instability needs to be examined. The Görtler vortex structure on concave walls and vortex breakdown of high intensity swirling flows are two examples of centrifugal instability. The swirl intensity or degree of swirl in a jet is characterized by swirl number (Eq. (11)). The effect of weak swirl ($S \leq 0.4$) is to increase the width of a free or confined jet flow: the enhancement rate in jet growth, entrainment, and decay is improved progressively as the degree of swirl increases. For high intensity swirl ($S \geq 0.6$), strong radial and axial pressure gradients are set up near the nozzle exit, resulting in axial recirculation in the form of a central toroidal recirculation zone, which is also known as vortex breakdown [11]. With these fundamental flow phenomena that govern the evolution of a rectangular jet, the computational results for a swirling shear layer emerging from an under-expanded supersonic rectangular nozzle may be presented.

5.1 Free jet from the plane rectangular nozzle with swirling shear layer

The instantaneous centerline static pressure distributions for plane rectangular nozzles with and without shear layer swirl are plotted in Figure 4. It is observed that the first shock is stronger and the second and third shocks are weaker for the case of shear layer swirl (30° swirl). We note that the addition of boundary layer swirl does not affect the shock spacing along the jet centerline. After the third shock cell where the flapping oscillation appears, the comparison between the results is not meaningful since both results are obtained from the instantaneous solutions.

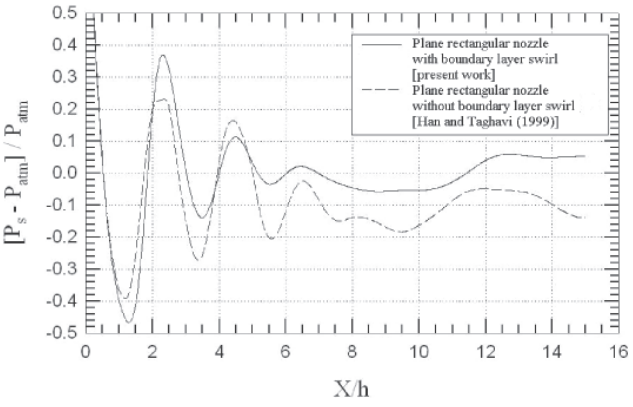

Fig. 4: Nozzle centerline static pressure distributions at the phase-locked moment in the axial direction for the plane rectangular nozzles with and without boundary layer swirl [13]

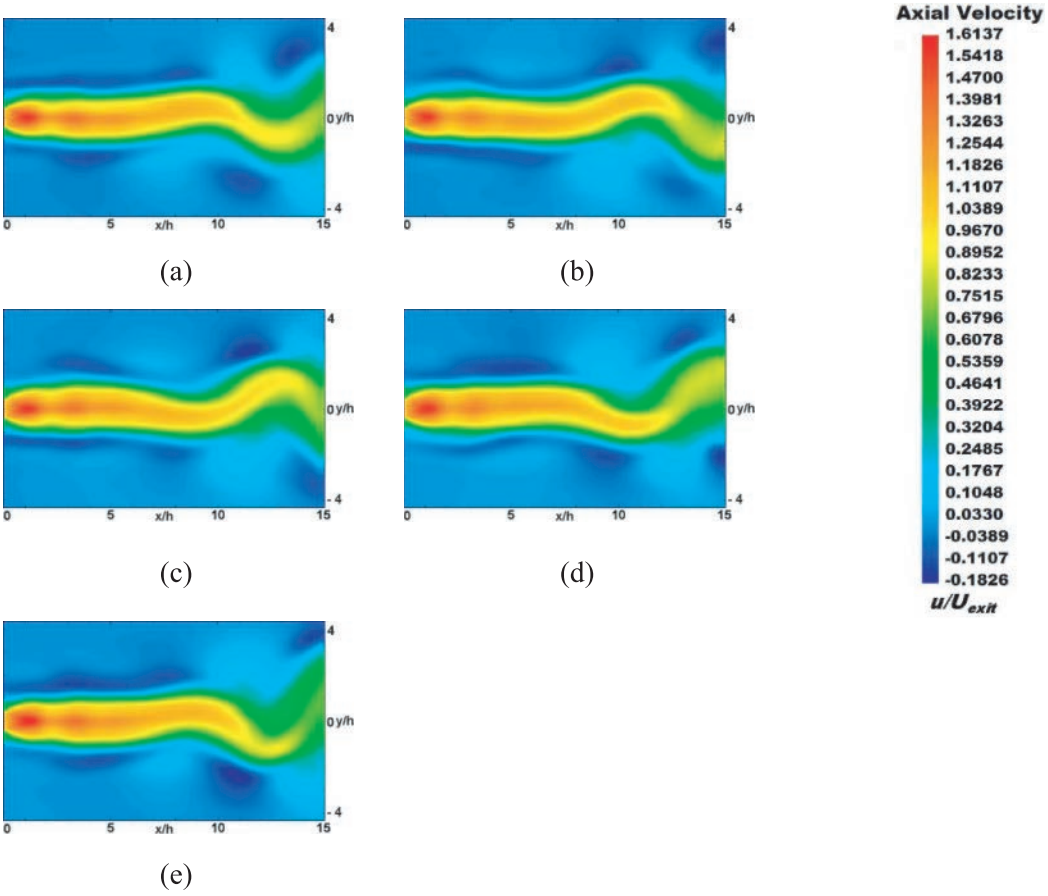

Fig. 5: The flapping oscillation mode ($f \approx 15$ kHz, $St \approx 0.754$) of jet at the center plane represented by axial velocity maps for the plane rectangular nozzle with boundary layer swirl. Phase difference from frame to frame is 90°. Parts (a)–(e) represent one full cycle of flapping oscillation mode viewed from nozzle's small dimension.

The axial velocity contour maps shown in Figure 5 are taken at the jet center plane (viewed from nozzle's small dimension), which clearly show one full cycle of flapping oscillation process of supersonic jet from the plane rectangular nozzle with shear layer swirl with frames at 90° phase difference (physical time step interval of about 1.68×10^{-5} s). The computational results for the case of plane rectangular nozzle with boundary layer swirl shows the frequency of this flapping oscillation mode at about 15,000 Hz, which is nearly twice the frequency of the non-swirling case [13]. Additional investigation on flowfields along the supersonic jet shows that low velocity fields are induced alternatively at each side of jet and travelled with the jet in the downstream direction.

The non-dimensional frequency of flapping oscillation mode shown in Figure 5 may be expressed as Strouhal number, which is a dimensionless parameter, used in oscillatory flows and is defined as:

$$St = f.D_{eq}/U_{exit} \tag{12}$$

where

$$D_{eq} = \sqrt{4wh/\pi} \tag{13}$$

where D_{eq} is the equivalent (or hydraulic) diameter calculated as 0.01512 m. The mass-averaged axial mean velocity at the nozzle exit, U_{exit}, is calculated to be 300.79 m/s based on speed of sound calculation for $T_{exit} = 249.85$ K. The axial velocity component in the swirling boundary layer is also assumed to correspond to the choked flow condition at the nozzle exit with Mach number of 1.0. Thus, Strouhal number for the flapping oscillation mode is calculated to be: $St_{flapping} \approx 0.754$.

In Figures 6(a) through 6(e), static pressure contour maps with frames at 90° phase difference (physical time step interval of about 1.68×10^{-5} s) for one full cycle of jet flapping oscillation mode ($f \approx 15{,}000$ Hz, $St_{flapping} \approx 0.754$) at the center plane viewed from nozzle's small dimension are presented. The figure shows that high pressure contours reside alternatively at each side of the jet after the

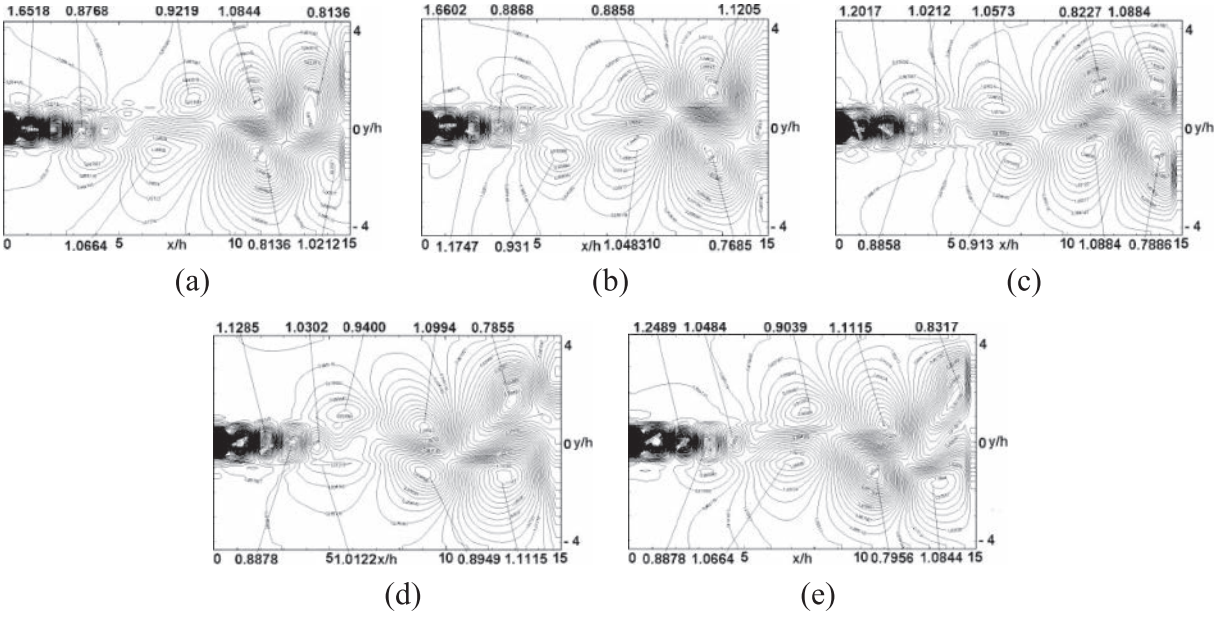

Fig. 6: The flapping oscillation mode ($f \approx 15$ kHz, $St \approx 0.754$) of jet at the center plane represented by static pressure maps for the plane rectangular nozzle with boundary layer swirl. Phase difference from frame to frame is 90°. Parts (a)–(e) represent one full cycle of flapping oscillation mode viewed from nozzle's small dimension.

second shock location and travel in the downstream direction with time.

A series of axial velocity contour maps with the phase difference of 90° between frames (time step interval of about 1.68×10^{-5} s) at the center plane viewed from nozzle's large dimension for one full cycle of jet spanwise oscillation for the plane rectangular nozzle with boundary layer swirl are shown in Figures 7(a) through 7(e) with the frequency of about 15,000 Hz, (with corresponding $St_{spanwise} \approx 0.754$). In these figures, the jet flowfield affected by shear layer swirl is spreading out more widely than the case without boundary layer swirl [13]. The supersonic jet from the plane rectangular nozzle with boundary layer swirl shown in Figure 7 also shows the symmetrical oscillation mode with the potential core expanding and contracting alternately as time elapses. In addition, it is also found that the rings formed inside potential core are bursting out alternately side by side along with the symmetrical oscillation. In Figure 7, two full cycles of symmetrical mode can be identified with 180° phase difference between frames. The frequency of symmetrical oscillation mode from Figure 7 is calculated to be about 30,000 Hz (with corresponding $St_{symmetrical} \approx 1.508$), which is twice the frequency of flapping or spanwise oscillation mode as shown in Figures 5 and 7. This phenomenon is the same as the case without shear layer swirl as reported by Han and Taghavi [13] and in the experimental results performed by other researchers [27, 32].

Static pressure contour maps at the center plane viewed from nozzle's large dimension for one full cycle of jet spanwise oscillation process from the plane rectangular nozzle with boundary layer swirl are showing in Figures 8(a) through 8(e) with the frames of 90° phase differences (physical time step interval of about 1.68×10^{-5} s). As in Figure 7, the frequency of spanwise oscillation mode is about 15,000 Hz and the corresponding Strouhal number is $St_{spanwise} \approx 0.754$. We observe the static pressure contours for two shock cells and the traveling low pressure contours after the location of $x/h \approx 8.0$. The low pressure contours located alternately side by side after $x/h \approx 8.0$ are responsible for the jet spanwise oscillation in the direction of nozzle's large dimension. In addition, it is also found from Figure 8 that just after $x/h \approx 4.0$ relatively higher static pressure contours reside below nozzle centerline ($z/h = 0$) in Figure 8(a), spread out to upper side in Figure 8(b), and reside above nozzle centerline in Figure 8(c) as time elapses. Again those relatively higher static pressure contours are forming below nozzle centerline in Figure 8(d) and spreading out to upper side in Figure 8(e). From such observation it can be noticed that such flow characteristics may be one of factors which induce jet spanwise oscillation. The spanwise oscillation mode of under-expanded supersonic jet in the direction of nozzle's large dimension is not detected in the case of plane rectangular nozzle without boundary layer swirl [13]. Thus we conclude that the span-

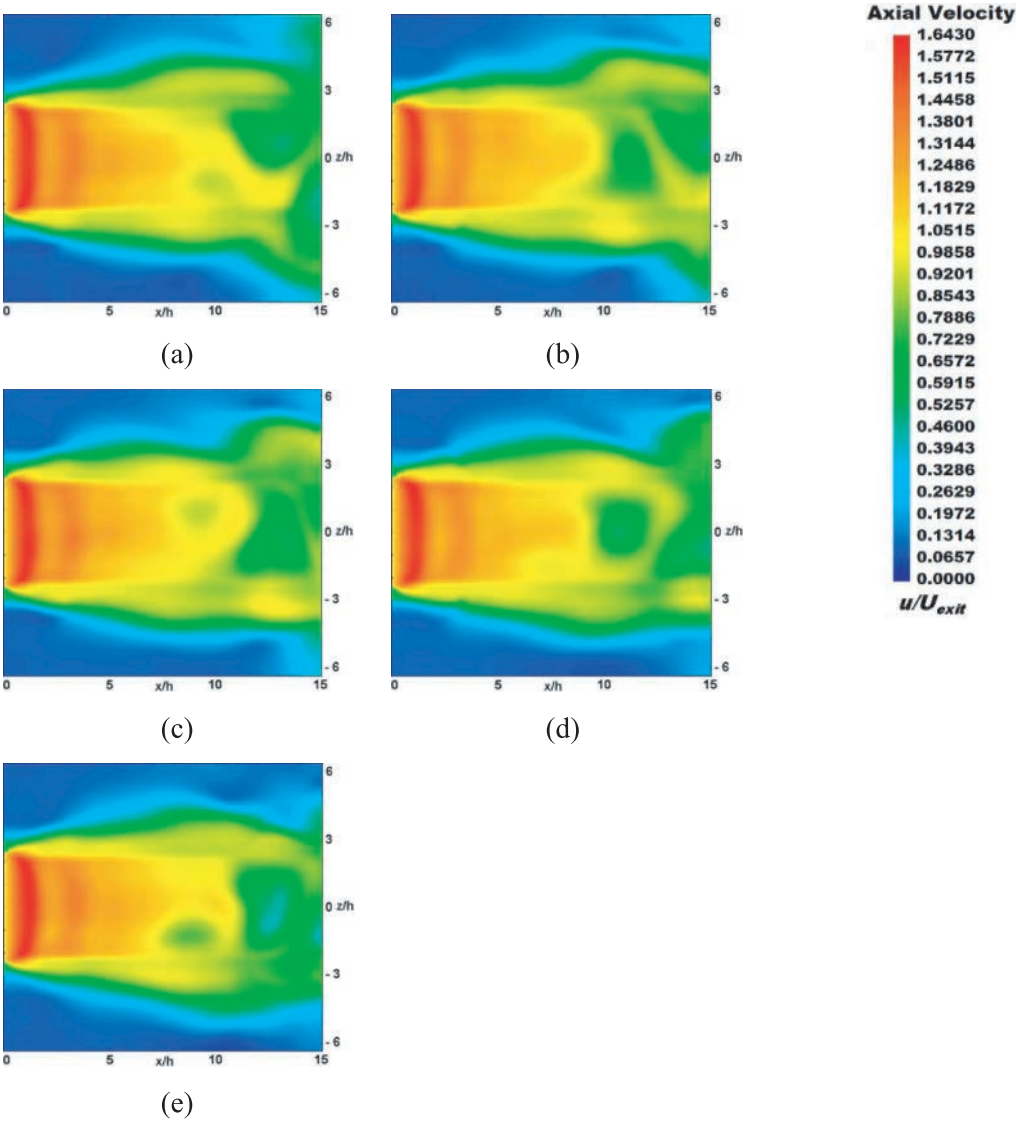

Fig. 7: The spanwise ($f \approx 15$ kHz, $St \approx 0.754$) and symmetrical ($f \approx 30$ kHz, $St \approx 1.508$) oscillation modes of jet at the center plane represented by axial velocity maps for the plane rectangular nozzle with boundary layer swirl. Phase differences from frame to frame are 90° for the spanwise oscillation mode and 180° for the symmetrical mode. Parts (a)–(e) represent one full cycle of spanwise oscillation mode and two full cycles of symmetrical mode viewed from nozzle's large dimension.

wise oscillations of rectangular jet in the direction of large nozzle dimension are induced by swirl in the jet shear layer.

Additionally, comparing to our previous results [13], we note that the jet width with boundary layer swirl is thinner in the small dimension (Figure 5) and larger in the large dimension (Figure 7) as compared with the same jet without shear layer swirl. Therefore, it is concluded that the jet with boundary layer swirl shows more active flapping, spanwise, and symmetrical oscillation modes than the case without boundary layer swirl. In addition, the axial thrust penalty for the proposed passive control of the plane rectangular nozzles through boundary layer swirl is limited to nearly 5.1% due to the reduction in axial velocity component in the boundary layer.

5.2 Free jet from the notched rectangular nozzle with swirling shear layer

A shock adaptive grid generator detects one strong shock for free jet from the notched rectangular nozzle with 30° swirl in the inner boundary of the nozzle exit and generates a shock adaptive grid system as shown in Figure 2(b).

The normalized nozzle centerline instantaneous static pressure distribution in the axial direction for the

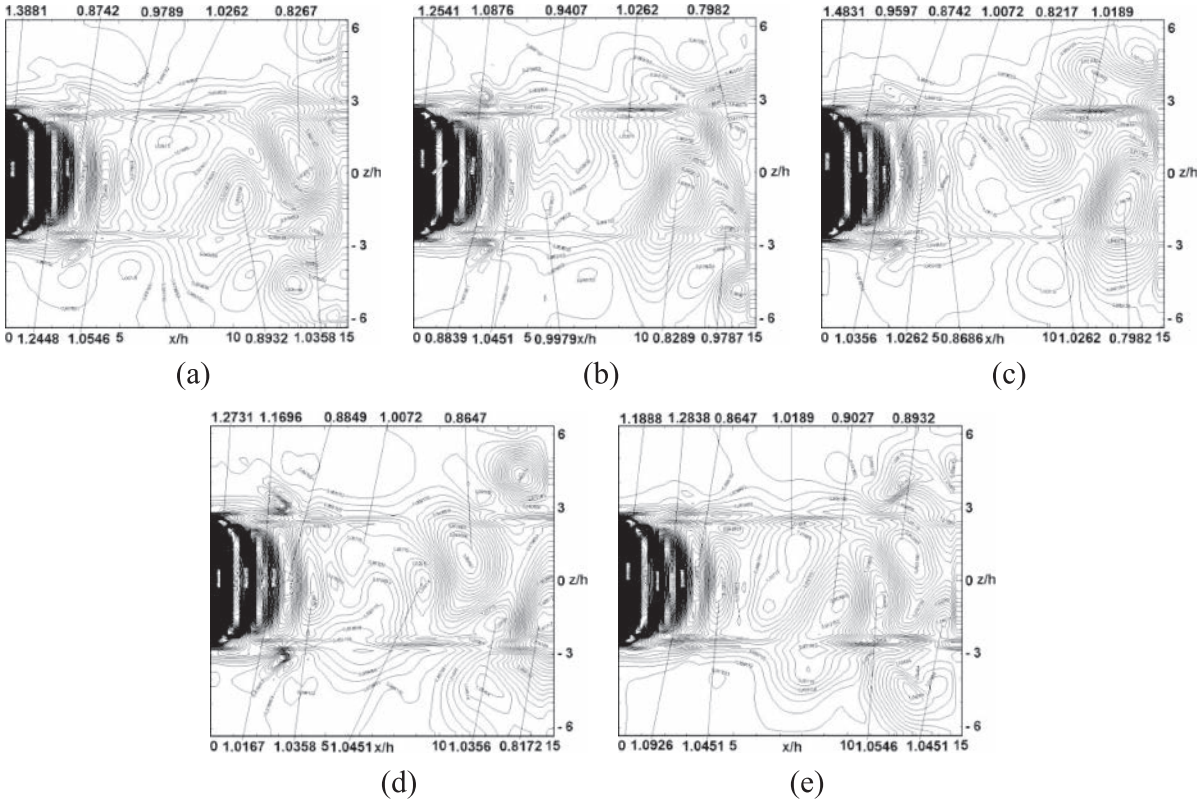

Fig. 8: The spanwise oscillation mode ($f \approx 15$ kHz, $St \approx 0.754$) of jet at the center plane represented by static pressure maps for the plane rectangular nozzle with boundary layer swirl. Phase difference from frame to frame is 90°. Parts (a)–(e) represent one full cycle of spanwise oscillation mode viewed from nozzle's large dimension.

notched rectangular nozzle with boundary layer swirl is shown in Figure 9 together with the previous computational results for the notched rectangular nozzle without boundary layer swirl [12]. This figure indicates that the flowfield contains only one strong shock that appeared at the nozzle centerline. After the first shock, the static pressure for the case with boundary layer swirl becomes much lower than for the case without boundary layer swirl indicating strong mixing enhancement due to shear layer swirl. Therefore, we conclude that the major contribution of the shear layer swirl in mixing enhancement in the notched nozzle configuration case takes place after the first shock.

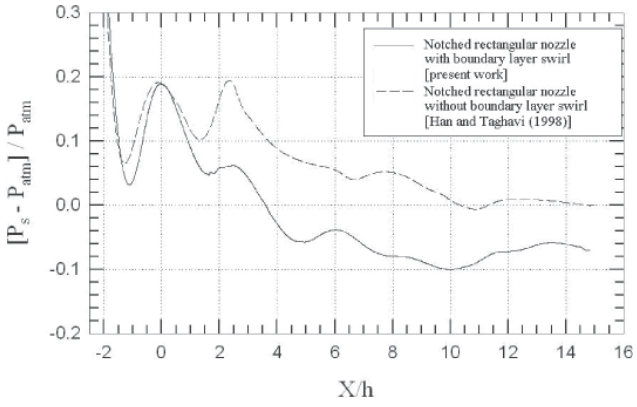

Fig. 9: Comparison of centerline static pressure distribution in the axial direction for the notched rectangular nozzles with and without boundary layer swirl [12]

Figures 10(a) through 10(e) represent axial velocity contour maps taken at the center plane viewed from nozzle's small dimension, which clearly show half a cycle of flapping oscillation process with frames at 45° phase differences (physical time step interval of about 4.4×10^{-5} s). The computation for the case of notched rectangular nozzle with boundary layer swirl shows the frequency of this flapping oscillation mode to be about 2,800 Hz. The frequency of flapping oscillation mode is somewhat lower than the frequency of the case without boundary layer swirl, which has the frequency of about 3,000 Hz [12].

The flapping oscillation mode observed in the notched rectangular nozzle jet with boundary layer swirl shown in Figure 10 can be also expressed as Strouhal number by considering the enlarged exit flow area due to notches

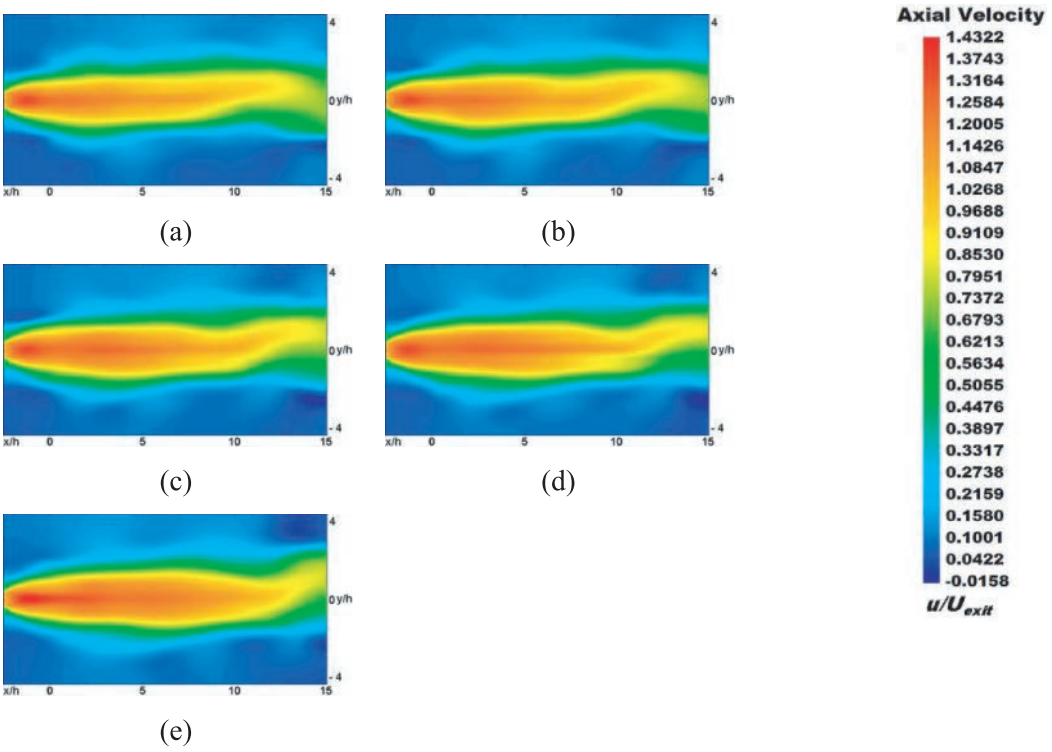

Fig. 10: The flapping oscillation mode ($f \approx 2.8$ kHz, $St \approx 0.167$) of jet at the center plane represented by axial velocity maps for the notched rectangular nozzle with boundary layer swirl. Phase difference from frame to frame is 45°. Parts (a)–(e) represent half a cycle of flapping oscillation mode viewed from nozzle's small dimension.

with the following equivalent diameter:

$$D_{eq} = \sqrt{4wh/(\pi \cos 45°)} \tag{14}$$

which gives the equivalent diameter of $D_{eq} = 0.01799$ m. In addition, the mass-averaged axial mean velocity at the nozzle exit, U_{exit}, is calculated as 301.34 m/s by considering the notch configuration at the nozzle exit, the speed of sound at $T_{exit} = 249.85$ K, the axial component of swirl velocity in the boundary layer, and the choked flow at the nozzle exit (i.e., Mach number of 1.0). Thus Strouhal number for the flapping oscillation mode is determined to be: $St_{flapping} \approx 0.167$.

Static pressure contour maps for half a cycle of jet flapping oscillation process at the center plane from nozzle's small dimension are presented in 45° phase interval frames of Figure 11 (physical time step interval of about 4.4×10^{-5} s). Figure 11 indicates that high pressure contours are induced alternately at each side of nozzle centerline after $x/h \approx 11.0$ and travel downstream as time elapses, which is responsible for the jet's flapping oscillation ($f \approx 2{,}800$ Hz, $St_{flapping} \approx 0.167$). When we observe static pressure contours in Figure 11, it can be found that one shock cell has been formed just at the nozzle exit where $x/h = 0$. In addition, after $x/h \approx 11.0$, it is also noticed that relatively higher static pressure contours reside above the nozzle centerline ($y/h = 0$) in Figure 11(a) and below the centerline in Figure 11(e), which make jet oscillate as time elapses.

A series of axial velocity contour maps at the center plane viewed from nozzle's large dimension, for half cycle of jet spanwise oscillation, from the notched rectangular nozzle with boundary layer swirl are presented in Figures 12(a) through 12(e). Each frame has 45° phase difference (physical time step interval of about 4.4×10^{-5} s). The figure shows the spanwise oscillation of jet in the direction of nozzle's large dimension due to the effect of notch in the nozzle exit and swirl in the nozzle exit boundary layer. The frequency of this spanwise oscillation is calculated to be about 2,800 Hz which is the same as the frequency of flapping oscillation mode. Also this spanwise oscillation mode observed in the notched rectangular jet with boundary layer swirl shown in Figure 12 can be expressed as Strouhal number of $St_{spanwise} \approx 0.167$.

Figure 13 shows the static pressure contour maps at the jet center plane viewed from nozzle's large dimension for half spanwise oscillation cycle for the notched rectangular nozzle with boundary layer swirl with frames of 45°

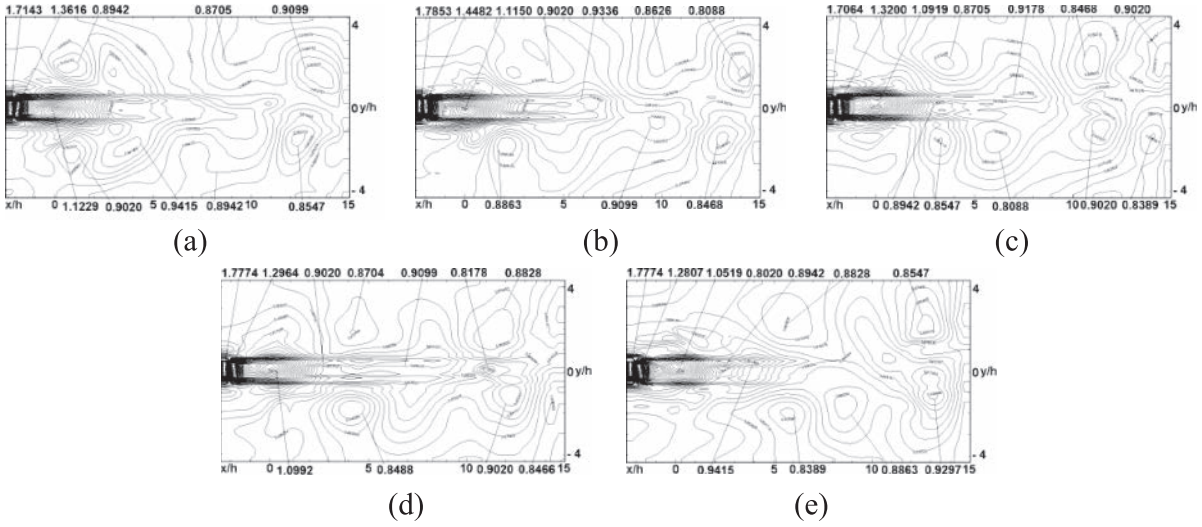

Fig. 11: The flapping oscillation mode ($f \approx 2.8$ kHz, $St \approx 0.167$) of jet at the center plane represented by static pressure maps for the notched rectangular nozzle with boundary layer swirl. Phase difference from frame to frame is 45°. Parts (a)–(e) represent half a cycle of flapping oscillation mode viewed from nozzle's small dimension.

phase difference (physical time step interval of about 4.4×10^{-5} s). Only one shock cell is found in Figures 13(a) through 13(e) as indicated also in Figure 9. In Figure 13 both low and high pressure contours are located at the same axial distance across the nozzle centerline after the location of $x/h \approx 8.0$. This phenomenon indicates that the jet spanwise oscillation with the frequency of about 2,800 Hz ($St_{spanwise} \approx 0.167$) could be achieved in the direction of nozzle's large dimension due to boundary layer swirl induction. The spanwise oscillation of supersonic jet in the direction of nozzle's large dimension is also found in the case of notched rectangular nozzle without boundary layer swirl [12] which shows somewhat higher frequency. Thus, we conclude that the spanwise oscillation of jet in the direction of nozzle's large dimension is not affected significantly by the presence of shear layer swirl. In addition, the axial thrust penalty by the proposed passive control of notched rectangular nozzle flows through induced shear layer swirl is nearly 4.9%.

5.3 Mass flow rate

Along with three instability modes (flapping, spanwise, and symmetrical oscillation modes) observed from the axial velocity and static pressure contours of previous figures, the cross-sectional views of axial velocity contours at various downstream locations can shed light on jet's mixing enhancement characteristics, i.e., the spreading rate, due to induced shear layer swirl in under-expanded supersonic jets. Figures 14(a), 14(b), and 14(c) show the instantaneous cross-sectional axial velocity contour plots at $x/h = 0.1$, 7.5, 11.5 locations respectively in the case of plane rectangular nozzle with boundary layer swirl. It is clearly observed from these figures that the jet is spreading outward in the downstream direction and the shear layer swirl also makes the jet rotate in the counter-clockwise direction (i.e., in the same direction as the induced swirl at the nozzle exit). We also note that the boundary layer swirl that is induced in the nozzle starts affecting the jet evolution immediately downstream of the nozzle exit. Comparing these figures (i.e., Figures 14(a) through 14(c)) to the case of non-swirling shear layer [13], which are shown in Figures 14(d) through 14(f), we can clearly discern the impact of boundary layer swirl on turbulent jet spreading and mixing enhancement. The coupling between the rectangular jet instability modes (i.e, flapping, spanwise and symmetrical) and the helical instability due to swirl is the physical driver for enhanced mixing and spreading rate in the jet.

The instantaneous cross-sectional axial velocity contour plots, for the case of notched rectangular nozzle with boundary layer swirl, at $x/h = 0.1$, 7.5, 11.5 locations are shown in Figures 15(a), 15(b), and 15(c) respectively. The jet spreading rate is clearly shown in the above figures with the combined effects of nozzle exit notch and boundary layer swirl. We observe that the jet is again rotating in the counter-clockwise direction (i.e., in the same direction as the induced swirl) due to the boundary layer swirl and the jet is spreading further outward diagonally as the jet evolves downstream. Again it is clearly seen that the shear layer swirl impacts the evolution of the rectangular jet im-

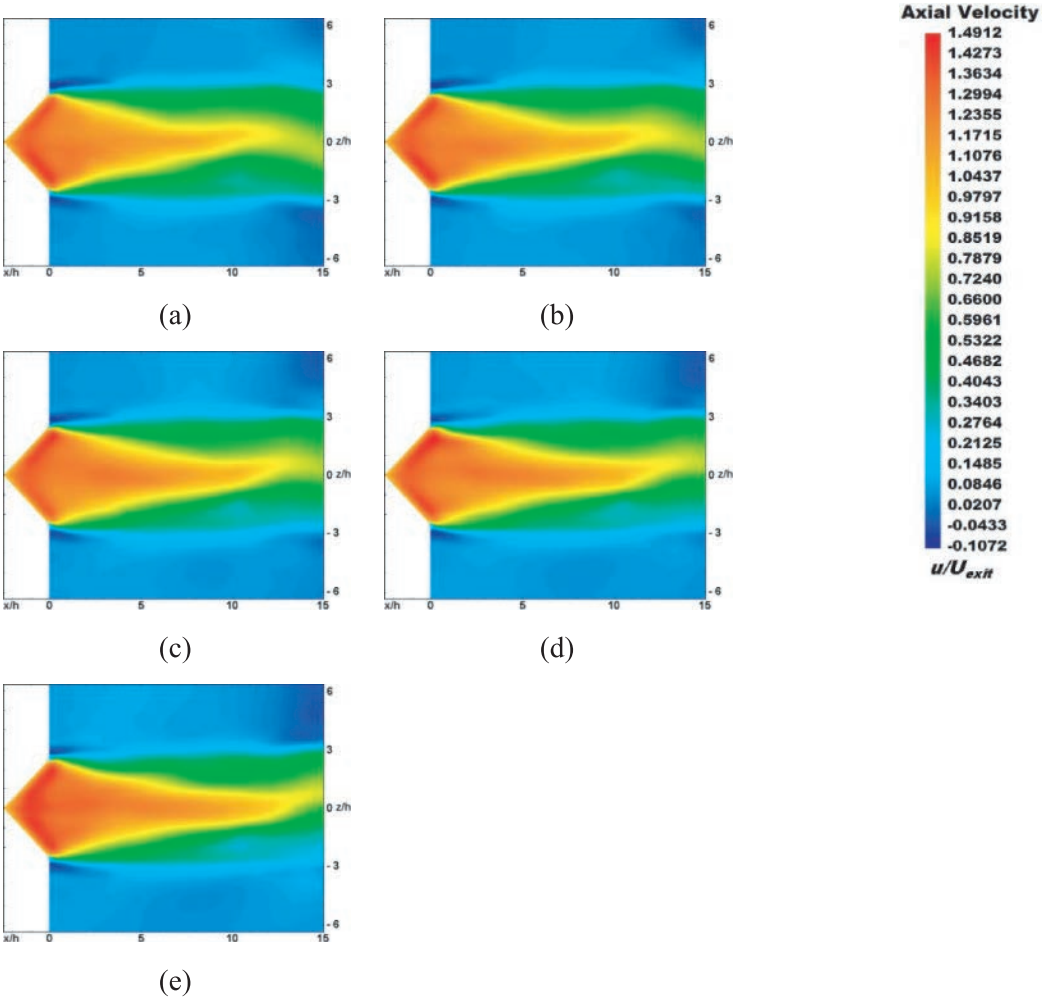

Fig. 12: The spanwise oscillation mode ($f \approx 2.8$ kHz, $St \approx 0.167$) of jet at the center plane represented by axial velocity maps for the notched rectangular nozzle with boundary layer swirl. Phase difference from frame to frame is 45°. Parts (a)–(e) represent half a cycle of spanwise oscillation mode viewed from nozzle's large dimension.

mediately downstream of the nozzle. Figures 15(d) through 15(f) show the instantaneous axial velocity contours at the same locations for the case of notched rectangular nozzle without boundary layer swirl [12]. The direct comparison points to the favorable effect of the boundary layer swirl on the jet spreading rate and mixing enhancement, thus serving as an effective (passive) control means of the supersonic jet.

The mixing enhancement achieved through boundary layer swirl for the plane rectangular nozzle is plotted in Figure 16 as the normalized mass flow rate distributions in the axial direction. It is seen that the mass flow rate increases by nearly 25% at 12 nozzle heights downstream of the nozzle with boundary layer swirl. Therefore, the jet entrainment and mixing is enhanced by the induced swirl in the shear layer primarily due to coupling of the jet instability modes with the helical instability due to swirl.

In Figure 17, the normalized mass flow rate distributions for the notched rectangular nozzle with and without boundary layer swirl are plotted in the axial direction. From this figure we can see that again the mixing enhancement is achieved through boundary layer swirl for the case of notched rectangular nozzle. It is also shown in this figure that the mass flow rate increases by nearly 41% at 8 nozzle heights downstream of the notched exit with boundary layer swirl, which again indicates the strong influence of boundary layer swirl, essentially instability mode coupling, on the jet entrainment and mixing.

Therefore, the mixing enhancement and control that is achieved through induced boundary layer swirl in under-expanded supersonic rectangular jets is significant while the penalty in gross thrust is relatively small. The physical mechanism can be attributed to the coupled centrifugal or helical instability due to swirl and rectangular

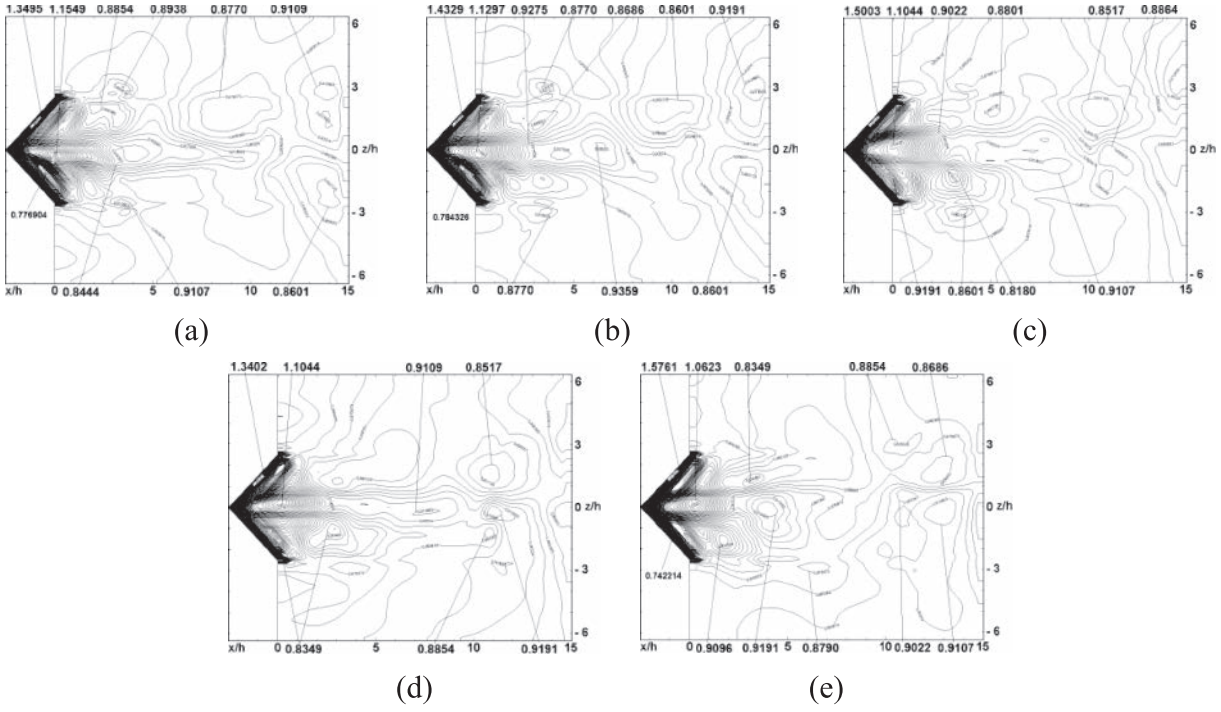

Fig. 13: The spanwise oscillation mode ($f \approx 2.8$ kHz, $St \approx 0.167$) of jet at the center plane represented by static pressure maps for the notched rectangular nozzle with boundary layer swirl. Phase difference from frame to frame is 45°. Parts (a)–(e) represent half a cycle of spanwise oscillation mode viewed from nozzle's large dimension.

jet instability of flapping, spanwise and symmetrical oscillations. The axial gross thrust penalty is about 5.1% for the plane rectangular nozzle and about 4.9% for the notched rectangular nozzle due to induced swirl in the nozzle exit boundary layer.

6 Conclusions

A three-dimensional unsteady Reynolds-Averaged Navier-Stokes (RANS) code was successfully used as a computational tool with Baldwin-Lomax and Chien k-ε turbulence models to study the macroscopic behaviors of coupled jet instabilities and mixing characteristics of under-expanded supersonic jets emerging from both plane and 45° notched rectangular nozzles (aspect ratio = 5; fully expanded jet Mach number = 1.526) with nozzle exit boundary layer swirls (30° swirl; $S = 0.41$). The three-dimensional instability characteristics of rectangular jets such as flapping, spanwise, and symmetrical oscillation modes were simulated using the unsteady capability of code. For the case of jet emerging from the plane rectangular nozzle with boundary layer swirl, the helical instability due to swirl affected the flapping oscillation and was observed with the frequency of about 15,000 Hz as viewed from nozzle's small dimension. The spanwise oscillation mode was found in nozzle's large dimension at the same frequency as the flapping oscillation mode. The symmetrical oscillation was also observed in nozzle's large dimension. The frequency of symmetrical oscillation mode was twice as much as the frequency of flapping or spanwise oscillation mode. The results for the notched rectangular nozzle with boundary layer swirl showed the flapping oscillation mode at the frequency of about 2,800 Hz in nozzle's small dimension. Also the spanwise oscillation mode viewed from nozzle's large dimension was found at the same frequency as the flapping oscillation mode.

A 30° boundary layer swirl induced at the nozzle exit excited centrifugal or helical instability modes in the shear layer and thus promoted jet mixing. The mass flow rate in the jet increased by nearly 25% at 12 nozzle heights downstream of the plane rectangular nozzle and by 41% at 8 nozzle heights for the notched rectangular nozzle. The significant mixing enhancement in the jet with boundary layer swirl at the nozzle exit is accomplished while the gross thrust penalty was modest at nearly 5.1% for the plane rectangular nozzle and about 4.9% for the notched rectangular nozzle.

Therefore, it can be concluded from analysis on the macroscopic behavior of jet instabilities and mixing characteristics that the applied passive jet excitation control method – boundary layer swirl at the nozzle exit – is an

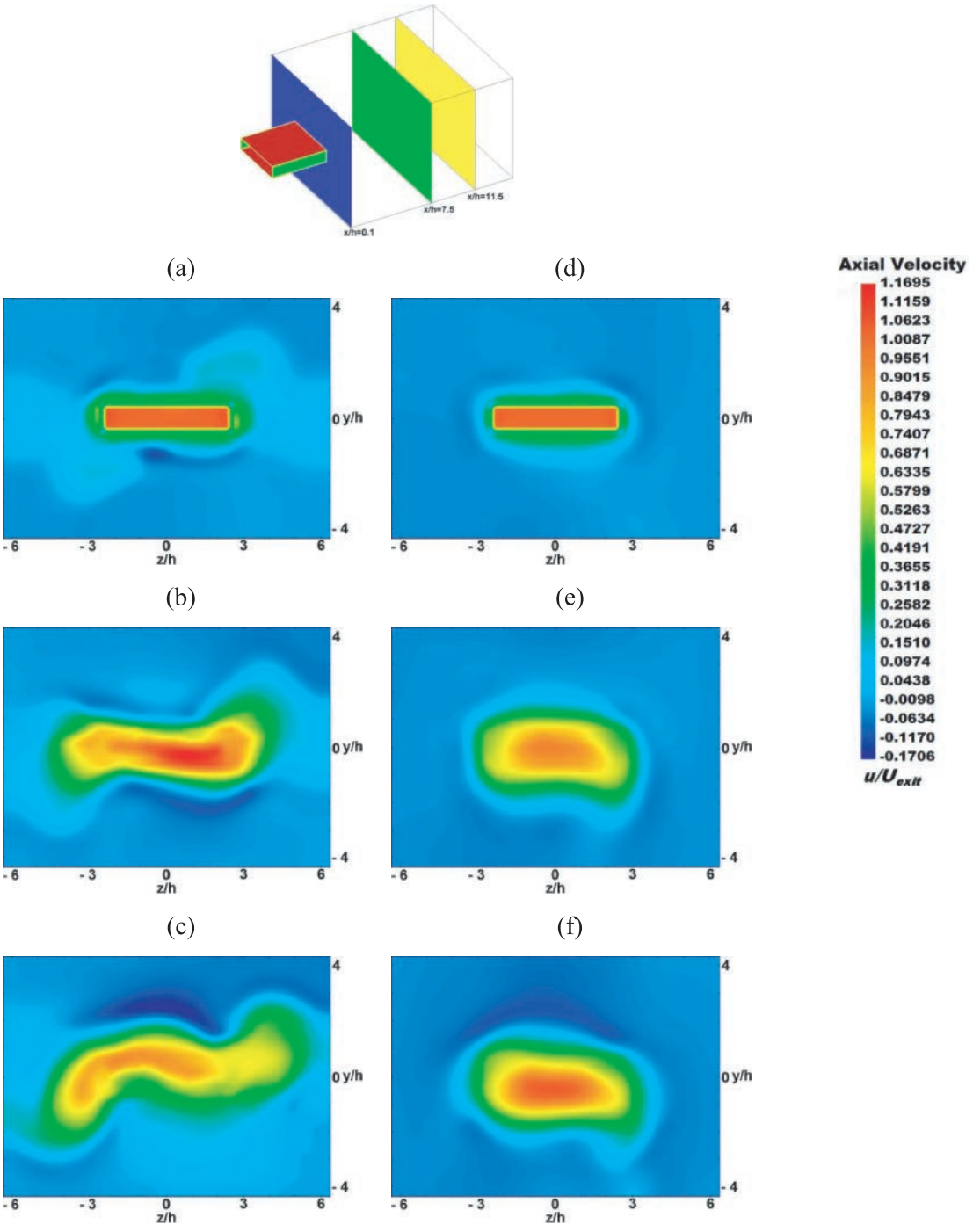

Fig. 14: Instantaneous axial velocity contour plots at the downstream locations of plane rectangular nozzle: (a–c) with boundary layer swirl [present work]; (d–f) without boundary layer swirl [13]

effective tool for the mixing enhancement of supersonic jets. The physical mechanism is traced to the coupled centrifugal and rectangular jet instability modes. In addition, it is found that a jet emerging from the notched rectangular nozzle shows better mixing enhancement than a jet from the plane rectangular nozzle when a boundary layer swirl at the nozzle exit is applied.

Nomenclature

AR	nozzle aspect ratio, w/h
CFL	Courant, Friedrichs, and Lewy number
D_{eq}	equivalent diameter, m
f	frequency, Hz
h	nozzle exit small dimension (height), m

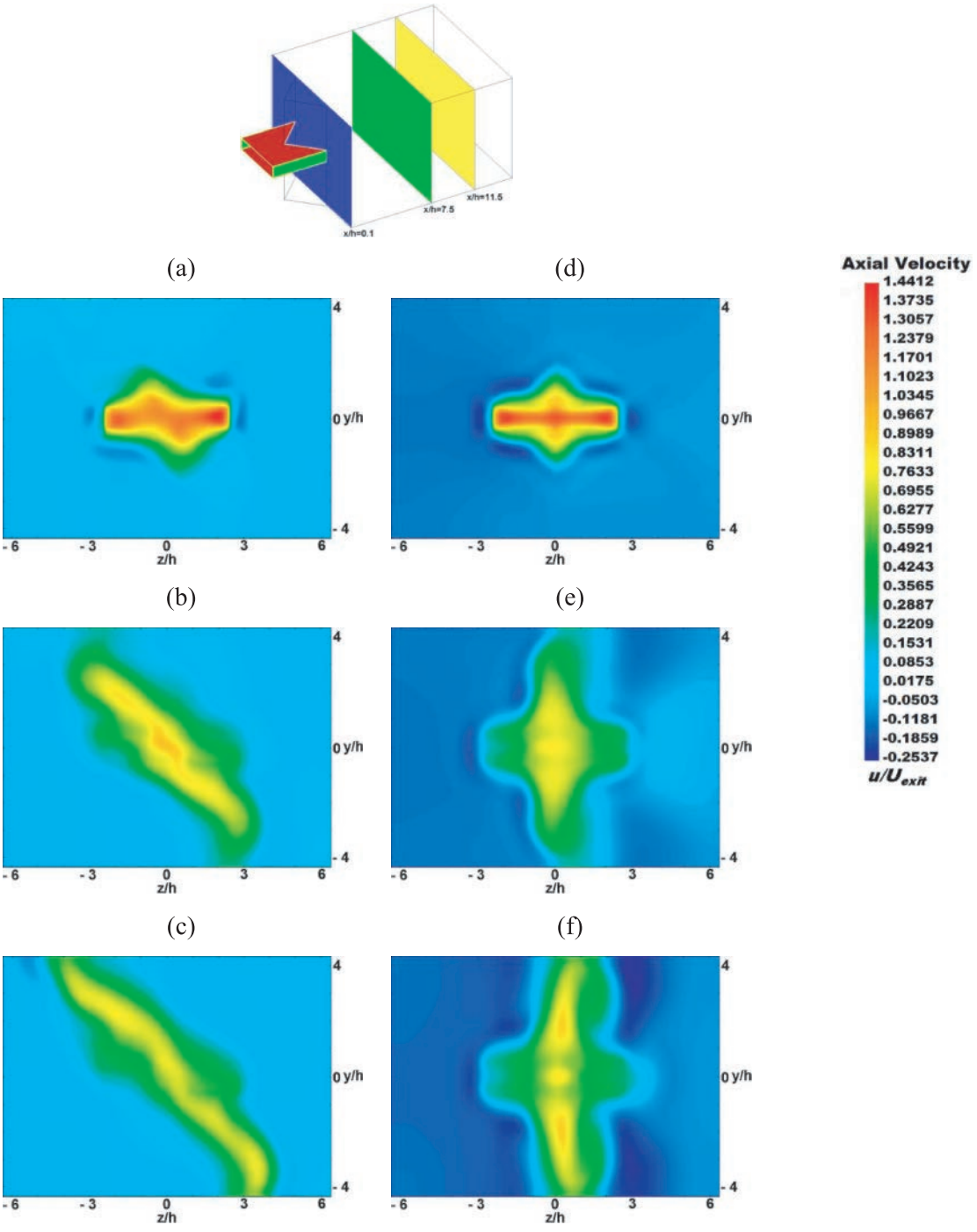

Fig. 15: Instantaneous axial velocity contour plots at the downstream locations of notched rectangular nozzle: (a–c) with boundary layer swirl [present work]; (d–f) without boundary layer swirl [12]

L	length, m	n	index
M	number of grid in y-direction	N	number of grid in x-direction
M_j	jet Mach number	p	index
m	instantaneous mass flow rate, kg/s; index	P	number of grid in z-direction
m_{exit}	mass flow rate at the nozzle exit, kg/s	P_{atm}	atmospheric pressure, N/m^2 (Pa)

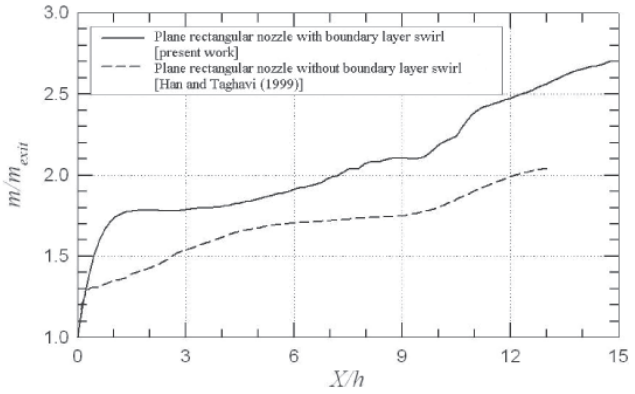

Fig. 16: Comparison of instantaneous mass flow rates in plane rectangular nozzles showing enhanced mixing/entrainment with boundary layer swirl

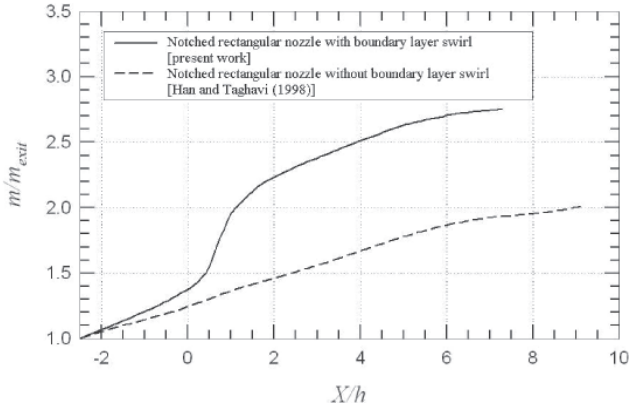

Fig. 17: Comparison of instantaneous mass flow rates in the notched rectangular nozzles showing enhanced mixing/entrainment with boundary layer swirl

P_s, p	static pressure, N/m^2 (Pa)
R_p	packing rate, %
s	index
S	degree of swirl
St	Strouhal number
T	static temperature, K
T_{exit}	nozzle exit static temperature, K
t	physical time, s
U_{exit}	axial mean velocity at the nozzle exit, m/s
u, v, w	velocity components in ξ, η, ζ-directions, m/s
w	nozzle exit large dimension (width), m
x, y, z	Cartesian coordinates in physical domain
$\varepsilon_E^{(2)}$, $\varepsilon_E^{(4)}$	the second-order and fourth-order explicit artificial viscosity
ε_I	implicit artificial viscosity
ξ, η, ζ	Cartesian coordinates in computational domain
θ	swirl angle, degree
φ	notch angle, degree

Acknowledgments: The authors' appreciation goes to Dr. Charles E. Towne from NASA-Glenn Research Center for providing the three-dimensional *Proteus* code and his help in running the code.

Received: February 27, 2013. Accepted: March 3, 2013.

References

[1] Baldwin BS, Lomax H (1978). Thin Layer Approximation and Algebraic Model for Separated Turbulent Flows. *AIAA Paper 78-257*.

[2] Bardina JE, Huang PG, Coakley TJ (1997). Turbulence Modeling Validation, Testing, and Development. *NASA TM 110446*.

[3] Basso E, Azevedo JLF (2004). Three-Dimensional Viscous Flow Simulations over the VLS Using Overset Grids. *Journal of the Brazilian Society of Mechanical Science and Engineering* 26(4): 439.

[4] Batchelor GK (1967). *An Introduction to Fluid Dynamics*. Cambridge University Press.

[5] Beam RM, Warming RF (1978), An Implicit Factored Scheme for the Compressible Navier-Stokes Equations. *AIAA Journal* 16(4).

[6] Behrouzi P, McGuirk JJ (2009). Effect of Tabs on Rectangular Jet Plume Development. *Journal of Propulsion and Power* 25(4): 930–939.

[7] Bodony DJ, Kim J, Freund JB (2011). Mechanisms of Jet Noise Reduction and Their Impact on Large-Eddy Simulations. *AIAA Paper 2011-20-411*.

[8] Camelli FE, Löhner R (2002). Combining the Baldwin Lomax and Smagorinsky Turbulence Models to Calculate Flows with Separation Regions. *AIAA Paper 2002-0426*.

[9] Chien KY (1982). Prediction of Channel and Boundary-Layer Flows with a Low-Reynolds Number Turbulence Model. *AIAA Journal* 20(1): 33–38.

[10] Frank JE (1994). Experimental Investigation of the Effect of Swirl on Mixing Enhancement of Supersonic Rectangular Jets. *M.S. Thesis*. The University of Kansas.

[11] Gupta AK, Lilley DG, Syred N (1984). *Swirl Flows*. Abacus Press, England.

[12] Han S, Taghavi R (1998). Supersonic Under-expanded Rectangular Jet Oscillations: A Computational Study. *Proceedings of the 21st International Congress on Aeronautical Sciences*. 13–18 September 1998, Melbourne, Australia, ICAS-98-2.10.5.

[13] Han S, Taghavi R (1999). Effects of Boundary Layer Swirl on Supersonic Under-expanded Rectangular Jet Oscillations. *AIAA Paper 99-0900*.

[14] Hussain F, Husain HS (1989). Elliptic Jets, Part 1. Characteristics of unexcited and excited jets. *Journal of Fluid Mechanics* 208: 257–320.

[15] Ibrahim MK, Nakamura Y (2000). The Effects of Vane-Type Tabs on Flow and Acoustic Fields of Supersonic Jet. *AIAA Paper 2000-0087*.

[16] Jameson A, Schmidt W, Turkel E (1981). Numerical Solutions of the Euler Equations by Finite Volume Methods Using Runge-Kutta Time-Stepping Schemes. *AIAA Paper 81-1259*.

[17] Kim CM, Krejsa EA, Khavaran A (1994). Significance of Shock Structure on Supersonic Jet Mixing Noise of Axisymmetric Nozzles. *AIAA Journal* 32(9): 1920–1923.
[18] Kim JH, Samimy M, Erskine WR (1998). Mixing Enhancement with Minimal Thrust Loss in a High Speed Rectangular Jet. *AIAA Paper 98-0696*.
[19] Kim JH, Samimy M (1999). Mixing Enhancement via Nozzle Trailing Edge Modifications in a High Speed Rectangular Jet. *Physics of Fluids* 11(9): 2731–2742.
[20] Kolbe RL, Kailasanath K, Boris JP (1996a). Numerical Studies of Heated Supersonic Rectangular Jets. *Proceedings of 1996 ASME Fluids Engineering Division Summer Meeting* 237: 523–528.
[21] Kolbe R, Kailasanath K, Young T, Boris J, Landsberg A (1996b). Numerical Simulations of Flow Modification of Supersonic Rectangular Jets. *AIAA Journal* 34(5): 902–908.
[22] Lo SC, Blaisdell GA, Lyrintzis AS (2011). Numerical Investigation of 3-D Supersonic Jet Flows using Large Eddy Simulation. *AIAA Paper 2011-1155-556*.
[23] Maciel ES (2008). Solutions of Inviscid and Viscous Flows using Structured High Resolution Algorithms in Three-Dimensions. *Proceedings of the 26th International Congress on Aeronautical Sciences*.
[24] McGuirk JJ, Rodi W (1977). The Calculation of Three-Dimensional Turbulent Free Jets. *Turbulent Shear Flows* 1: 71–83.
[25] Raman G (1996). Cessation of Screech in Under-expanded Jets. *AIAA Paper 96-1719*.
[26] Raman G (1998). Advances in Understanding Supersonic Jet Screech. *AIAA Paper 98-0279*.
[27] Raman G, Rice EJ (1994). Instability Modes Excited by Natural Screech Tones in a Supersonic Rectangular Jet. *Physics of Fluids* 6(12): 3999–4008.
[28] Raman G, Taghavi R (1998). Coupling of Twin Rectangular Supersonic Jets. *Journal of Fluid Mechanics* 354: 123–146.
[29] Rice EJ, Raman G (1993). Enhanced Mixing of a Rectangular Supersonic Jet by Natural and Induced Screech. *AIAA Paper 93-3263*.
[30] Sforza PM, Steiger MH, Trentacoste N (1966). Studies on Three-Dimensional Viscous Jets. *AIAA Journal* 4(5): 800–806.
[31] Steger JL (1978). Implicit Finite-Difference Simulation of Flow about Arbitrary Two-Dimensional Geometries. *AIAA Journal* 16(7): 679–686.
[32] Suda H, Manning TA, Kaji S (1993). Transition of Oscillation Modes of Rectangular Supersonic Jet in Screech. *AIAA Paper 93-4323*.
[33] Taghavi R, Rice EJ, Farokhi S (1988). Controlled Excitation of a Cold Turbulent Swirling Free Jet. *Journal of Vibration, Acoustics, Stress, and Reliability in Design* 110: 234–237.
[34] Towne CE, Schwab JR, Bui TT (1993). *Proteus* Three-Dimensional Navier-Stokes Computer Code – Ver. 1.0; Volume 1 – Analysis Description; Volume 2 – User's Guide; Volume 3 – Programmer's Reference. *NASA TM 106337*; *106340*; *106341*. NASA Glenn Research Center.